Korean J. Chem. Eng., 34(8), 2265-2274 (2017)
DOI: 10.1007/s11814-017-0110-5

pISSN: 0256-1115
eISSN: 1975-7220

Equilibrium and kinetic studies of azo dye (Basic Red 18) adsorption onto montmorillonite: Numerical simulation and laboratory experiments

Shabnam Hasani*,†, Faramarz Doulati Ardejani*,†, and Mohammad Ebrahim Olya**

*School of Mining, College of Engineering, University of Tehran, Tehran, Iran
**Department of Environmental Research, Institute for Color Science and Technology, Tehran, Iran
(*Received 16 December 2016 • accepted 12 April 2017*)

Abstract−Adsorption of BR 18 dye onto nano-clay adsorbent was investigated. Nano-clay was characterized by using FTIR, SEM, TEM, XRD and BET analysis. The percent removal increased by increasing nano-clay dose, while pH and stirring speed had no significant effect on the adsorption rate. It was observed that the uptake of dye onto nano-clay initially increased rapidly, and then decreased slowly until the equilibrium was reached. The adsorption capacity rose with an increase in temperature. Moreover, the adsorption kinetics was very fast and followed a pseudo second-order. The intra-particle diffusion was observed to be the rate-controlling step. In addition, equilibrium data fitted well with the Langmuir adsorption model. This paper also presents a numerical simulation incorporating the second-order kinetic expression using COMSOL Multiphysics software. The numerical modelling results and the experimental data were in excellent agreement.

Keywords: Computational Fluid Dynamics, COMSOL Multiphysics, Azo Dye, Adsorption, Montmorillonite

INTRODUCTION

Synthetic dyes are used widely in textile, paint, paper and printing industries. Wastewaters from textile industries comprise various pollutants, including a large amount of organic matter and color problem, depending upon the types of dyes, surface active materials and textile additives used in the process [1,2]. Generally, the dyes used in the textile industry include basic dyes, acid dyes, reactive dyes, direct dyes, azo dyes, mordant dyes, vat dyes, disperse dyes and sulfur dyes [3]. Azo dyes having one or more azo groups (-N=N-) in aromatic rings are considered to be the major type of dyes used in industry [3,4]. So, the removal of such dyes from industrial effluents should be considered in order to control water pollution and raise water quality.

The most widely applied techniques of dye removal from industrial effluents are categorized into three groups: chemical (e.g., oxidative processes), physical (e.g., adsorption) and biological (e.g., decolorization by white-rot fungi, adsorption by living/dead microbial biomass). Currently, the main focus is to find environmentally friendly and cost-effective physical and chemical methods of textile dye treatment [5-7]. Among the abundant methods of dye removal, adsorption is the best choice and gives appropriate results, as this method can be applied to remove different types of coloring materials. Recently, a number of methods have been investigated in developing the cheaper and effective adsorbents. Numerous researchers have proposed non-conventional inexpensive adsorbents, comprising natural materials [8-12], biomaterials [13], and waste materials from agriculture and industry [14]. Investigations have revealed that these materials could be effectively used as adsorbents to remove dyes from solution.

Clays are natural environment-friendly materials and are extensively used for the adsorption of the organic pollutants due to their high specific surface area, chemical and mechanical stabilities, high ion exchange capacity, swelling property and a variety of surface and structural properties. In addition, the most-used clays as nano-adsorbents include montmorillonite/smectite group and kaolinite group clays [15-21]. Among the various smectite minerals, montmorillonite is popularly utilized for modification purposes because of its high adsorption capacity and favourable surface properties [22]. So, raw and modified montmorillonite have been successfully used as adsorbents for various dyes such as Crystal violet [23], Disperse Blue 56 and Disperse Red 135 [24], Rhodamine B [25], Methylene blue [26], and Malachite green [27].

Adsorption process has been modelled by many researchers. According to Ardejani et al. (2007), a numerical model is a valuable tool which can provide insight into the adsorption process. A numerical model can predict future events. It may indicate which factor(s) in a real system are most important from a sensitivity view point. A model can help to design, optimize and predict the performance of field remediation and contaminated water treatment programs [28]. In a batch system, there is usually one transport mode and a major process occurring simultaneously, such as diffusion and chemical reactions involved in adsorption.

Finite element method (FEM) is mostly used for the modelling and simulation for solid mechanics problems. Besides, it is used for multiphysics modelling and simulation including computational fluid dynamics (CFD) [29,30]. In the present work, a novel solving technology called COMSOL Multiphysics, was employed to solve the partial differential equations of CFD models friendly and efficiently [31-33]. It involves diffusion transport and adsorption process.

†To whom correspondence should be addressed.
E-mail: fdoulati@ut.ac.ir, shabnamhasani@ut.ac.ir

In the present study, montmorillonite was used as a natural adsorbent for removal of Basic Red 18 dye from aqueous solution. Our aim was to determine the optimum conditions for removal of Basic Red 18 from a simulated wastewater. In addition, a computational fluid dynamics (CFD) model has been presented using COMSOL Multiphysics software to simulate Basic Red 18 dye removal from an aqueous solution. This model can provide useful data required for developing an appropriate treatment system based on adsorption process.

MATERIALS AND METHODS

1. Adsorbent Characterization

Measurement of the surface area of the nanoclay involved using standard Brunauer-Emmett-Teller (BET) analyzer (Belsorp mini-II). FTIR spectra were obtained using Nicolet Instrument crop., USA, spectrophotometer. Morphological features of samples were obtained using a scanning electron microscope (SEM, LEO1455VP, England), and transmission electron microscopy (TEM) techniques were carried out on the clay powder. To investigate the crystalline structure of the nanoclay, a X-ray diffractometer (Siemens D-500) was used.

2. Reagents and Solutions

BR 18 dye (analytical grade, $C_{19}H_{25}Cl_2N_5O_2$, λ_{max}=488 nm) was used without further purification. Distilled water was throughout used as solvent. For adsorption experiments, various concentrations of dye solutions ranging from 10 to 200 mg/L) were prepared. The pH adjustments of the solution were made by adding a slight amount of HCl or NaOH.

3. Batch Adsorption Procedure

The adsorption measurements were conducted by mixing various amounts of nanoclay (0.01-0.1 g) in jars comprising 200 mL of a dye solution (20 mg/L) and an agitating speed of 200 rpm at temperature 25±1 °C for 20 min to achieve equilibrium conditions. After adsorption experiments, the sorbent was separated from the solution by Hettich EBA20 centrifuge, and the concentration of dye was then determined. In the batch system, effects of the major independent parameters such as adsorbent dose, pH, stirring speed, dye concentration, contact time and temperature were studied and optimized.

4. Isotherm Studies

The isotherm experiments were carried out by changing the initial dye concentrations (C_0) from 100 to 200 mg·L^{-1} and shaking with 0.04 g adsorbent in 200 ml dye solution for an equilibrium time at a constant temperature of 25±1 °C. The initial pH of dye solutions was 4.8 and no adjustments were done on the pH after nanoclay addition. The equilibrium dye concentrations (C_e) were then measured and the quantities of dye adsorbed per unit weight of adsorbent (q_e) were calculated as follows [34]:

$$q_e = \frac{(C_0 - C_e)\cdot V}{M} \quad (1)$$

The adsorbate distribution between the liquid phase and solid phase was assessed by different isotherm models once the BR 18 uptake had reached equilibrium. Therefore, Langmuir, Freundlich, and Temkin isothermal models were applied to the experimental data obtained during the isothermal adsorption investigations.

4-1. Langmuir Isotherm

The well-known linear form of Langmuir equation (Eq. (2)), which was applied on the experimental data, can be expressed as follows [35]:

$$\frac{C_e}{q_e} = \frac{1}{Q_0 K_L} + \frac{1}{Q_0} C_e \quad (2)$$

where q_e denotes the amount of solute adsorbed per unit weight at concentration C (mg·g^{-1}), C_e represents the equilibrium concentration of the dye (mg·L^{-1}), Q_o is referred to the maximum adsorption capacity and K_L is Langmuir isotherm constant (L·mg^{-1}).

The equilibrium parameter, R_L, is a dimensionless constant [36], which is given by Eq. (3):

$$R_L = \frac{1}{1 + K_L C_0} \quad (3)$$

R_L shows the adsorption type to be unfavorable (R_L>1), linear (R_L= 1), favorable (0<R_L<1), or irreversible process (R_L=0) [36].

4-2. Freundlich Isotherm

Eq. (4) describes the Freundlich model for the adsorption of solutes from a aqueous phase to a solid surface which was used in this study [37]:

$$\log q_e = \log K_F + \left(\frac{1}{n}\right) \log C_e \quad (4)$$

where q_e denotes the amount of a solute adsorbed (mg·g^{-1}), C_e is the equilibrium concentration of the adsorbate (mg·L^{-1}), K_F and n represent the Freundlich constants, describing the adsorption capacity and adsorption intensity, respectively.

4-3. Temkin Isotherm

To evaluate the heat of adsorption of adsorbate molecules on the surface of adsorbent particles, the equilibrium data was attempted by applying a linear form (Eq. (5)) of Temkin equation [38].

$$q_e = k_1 \ln k_2 + k_1 \ln C_e \quad (5)$$

where q_e represents the solute quantity adsorbed at equilibrium (mg·g^{-1}), C_e denotes the dissolved concentration at equilibrium (mg·L^{-1}), k_1 is referred to the Temkin isotherm energy constant (L·mg^{-1}) associated with the heat of adsorption and k_2 is the Temkin's isotherm constant.

5. Kinetic Studies

The kinetic study was performed by measuring the concentration of the BR 18 solution at pre-set time intervals. The amount of the dye adsorbed at time t, q_t (mg·g^{-1}) can be calculated by applying Eq. (6):

$$q_t = \frac{(C_0 - C_t)V}{M} \quad (6)$$

where C_o and C_t (mg·L^{-1}) are the liquid-phase concentration of the dye at the initial and any time t, respectively; V(L) represents the volume of the solution; and M(g) denotes the mass of the dried adsorbent used [39]. Three kinetic models were used which are discussed below.

5-1. Pseudo-first-order Kinetic Model

The pseudo-first order equation of Lagergren can be expressed as:

$$\frac{dq_t}{dt} = k_1(q_e - q_t) \quad (7)$$

where q_t and q_e represent the amounts of BR 18 adsorbed (in mg·g^{-1}) at time t and equilibrium, respectively, and k_1 is the pseudo-first order rate constant for the adsorption process ($1 \cdot min^{-1}$) [40].

5-2. Pseudo-second-order Kinetic Model

The pseudo-second order kinetic equation describing the chemical adsorption process is given below:

$$\frac{dq_t}{dt} = k_2(q_e - q_t)^2 \quad (8)$$

where k_2 represents the equilibrium rate constant of pseudo-second order equation ($g \cdot mg^{-1} \cdot min^{-1}$) [41].

5-3. Intraparticle Diffusion Model

The adsorption of solutes on an adsorbent is a two-step process: transport of solute from the boundary film to the external surface of the adsorbent which is termed film diffusion; transfer of solute from the surface to the interlayer space active sites. The external mass transfer resistance can be ignored with high agitation rate [42].

The interlayer diffusion equation can be expressed as follows [43]:

$$q_t = C_b + K_i\sqrt{t} \quad (9)$$

where q_t is the adsorbed quantity of BR 18, K_i denotes the interlayer diffusion parameter, and C_b represents the thickness of the boundary layer.

6. Adsorption Thermodynamics

The thermodynamic parameters including changes in standard enthalpy (DH^0), standard entropy (ΔS^0) and standard Gibbs free energy (ΔG^0) were determined to understand the nature of RB 18 adsorption by nanoclay.

The Gibbs free energy change can be calculated at constant temperature and from Van't Hoff equation applying Eqs. (10) and (11), respectively [44].

$$\Delta G^0 = -RT\ln K_d \quad (10)$$

where K_d represents the distribution constant at equilibrium, which is equivalent to q_e/C_e.

$$\Delta G^0 = \Delta H^0 - T\,\Delta S^0 \quad (11)$$

According to Eqs. (10) and (11), the distribution constant is related to the changes in the standard entropy, ΔS^0 and enthalpy, ΔH^0 as given by Eq. (12).

$$\ln K_d = \frac{\Delta S^0}{R} - \frac{\Delta H^0}{RT} \quad (12)$$

7. Adsorption Modelling

7-1. Mass Transport Equation

The governing partial differential equation for transport of a single solute in a saturated porous medium with considering the equation for the pollutant mass balance on the solid phase can be expressed as follows [45]:

$$\frac{\partial(\emptyset C)}{\partial t} = \nabla\cdot[\emptyset D\cdot\nabla C] - \nabla\cdot(u_l C) - \frac{\partial(\rho_s \emptyset_s q)}{\partial t} \pm \emptyset\rho Y \quad (13)$$

where Ø is the porosity, ρ denotes the aqueous phase density, C is the pollutant concentration, D is referred to the dispersion tensor, u_l is the Darcy velocity, q signifies the solute content adsorbed onto the porous media, ρ_s represents the density of the solid phase, $\emptyset_s$ denotes the volumetric fraction of the solid and Y is the rate of chemical interactions (sources or sinks).

Considering the diffusion mechanism in a batch system, Eq. (13) can be reduced as follows:

$$\frac{\partial C}{\partial t} = \nabla\cdot(D_{diff}\nabla\cdot C) - \frac{\rho_b}{\emptyset}\frac{\partial(q)}{\partial t} \pm \rho Y \quad (14)$$

where D_{diff} and ρ_b are the diffusion coefficient and the bulk density of solid [46].

7-2. Modelling Tool

Simulation using COMSOL Multiphysics contains six general steps: 1. Defining the governing equations and selection of spatial dimensions, 2. Creating the system geometry in software environment, 3. Determining the boundary condition, 4. Defining the physical properties and initial guesses, 5. Generating the mesh generation, selecting the necessary solver and solving the problem, 6. Post processing step and creating the results.

RESULTS AND DISCUSSION

1. Characteristics of Adsorbent

1-1. XRD Analysis

XRD is often used to determine the mineralogical structure of the raw material constituents as well as qualitative and quantitative phase analysis of multiphase mixtures [47]. XRD pattern of nanoclay sample is shown in Fig. 1. A sharp peak at approximately 7° (2θ) in the XRD pattern of adsorbent can be attributed to the (001) reflection of montmorillonite (Mt). A small peak at approximately 27° (2θ) as an impurity is attributed to quartz (Q). A peak at around 22° (2θ) is related to high-temperature form of cristobalite (β-Cristobalite).

The wavenumbers and assignments of the main vibration modes in the FTIR spectra of nanoclay (Fig. 2) were obtained. The characteristic band at ~3,630 cm^{-1} is related to the stretching vibration of structural OH (Al-OH). Vibration bands centered at ~1,639 cm^{-1} in montmorillonite are attributed to the bending vibrations of the adsorbed water [48]. The clay mineral spectra show a band at 1,036 cm^{-1}, associated with Si-O-Si stretching vibrations, a band at 624 cm^{-1} which signifies coupled Al-O and Si-O [49]. A broad band at 1,091 cm^{-1} is related to Si-O stretching vibrations. In addition, tet-

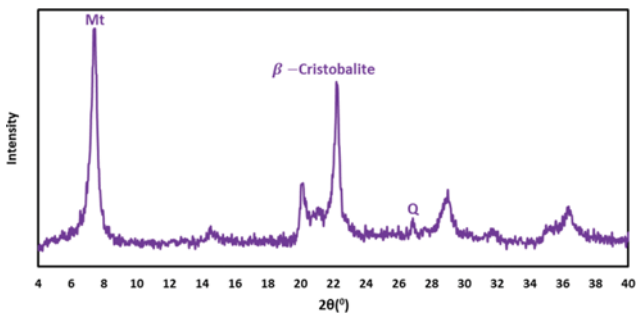

Fig. 1. XRD pattern of montmorillonite (Mt).

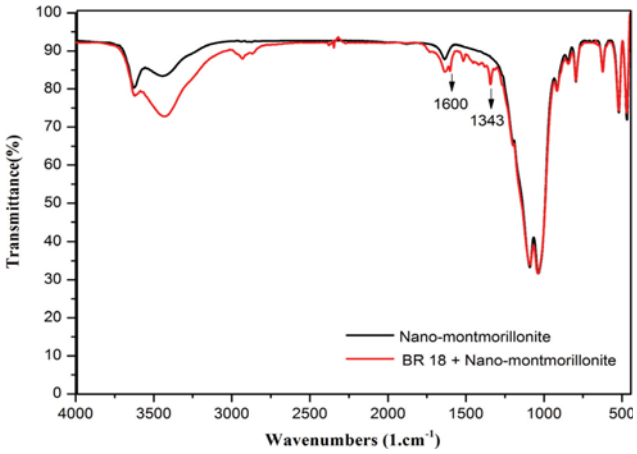

Fig. 2. FTIR spectra of the nanoclay, (top) before and (bottom) after adsorption of azo dye.

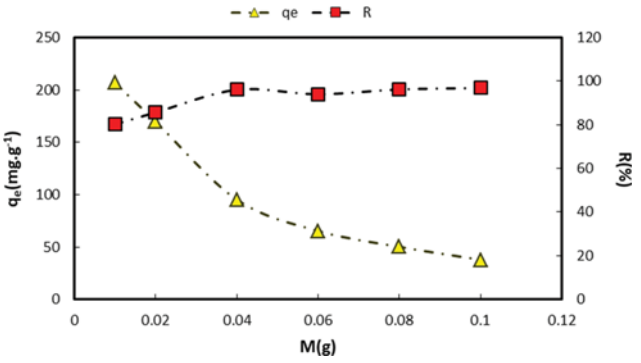

Fig. 4. Effect of adsorbent dosage on the removal of BR 18; q_e and R are the amount of equilibrium adsorption and the percent removal, respectively (Condition: pH=4.8, T=25±1 °C, C_0=20 mg L^{-1}, equilibrium time=20 min and stirring speed=200 rpm).

rahedral Si-O-Al and Si-O-Mg bending frequencies were at 520 and 470 cm^{-1}, respectively. The band at 796 cm^{-1} might be caused by the presence of amorphous silica in the clay minerals [23]. The presence of -OH groups on the surface of adsorbent has an important role for the adsorption of cationic species such as BR 18 [50].

New bands were observed at 1,600 cm^{-1} and 1,343 cm^{-1} after absorbing the BR 18. A peak at 1,600 cm^{-1} proves the presence of azo dye and a band at 1,343 cm^{-1} could be used as an evidence for adsorption of BR 18 on montmorillonite surface [51]. These bands could be related to CH bending and N-H bending vibrations.

The surface area of nanoclay was determined by BET method and a value of 49.5 $m^2 \cdot g^{-1}$ was calculated.

The morphology of montmorillonite can be seen in SEM image of Fig. 3(a). This figure shows uniformly layered structured with an ultrathin shelly. The TEM micrograph of the adsorbent (Fig. 3(b)) indicates the partial exfoliation of montmorillonite.

2. Effect of Adsorbent Dosage

Adsorption of BR 18 was conducted by adding 0.01-0.1 g of nanoclay to 200 mL of 20 $mg \cdot L^{-1}$ dye solution at a speed of 200 rpm with a temperature control of 25±1 °C for 20 minutes. At certain time intervals, the samples were taken and removed by centrifugation at a speed of 4,000 rpm for 5 min. The remaining concentration was determined spectrophotometrically at its corresponding λ_{max}.

The percentage of BR 18 absorption increased from 80.19 to 96.9%, as the nanoclay dose was increased from 0.01 g to 0.04 g/200 ml at equilibrium time (20 min). Further increase in adsorbent dosage from 0.04 to 0.1 g/200 ml did not enhance the removal percentage, so the optimum adsorbent was considered 0.04 g (Fig. 4). Increase in the removal percentage with increase in nanoclay content can be attributed to increased surface area and the availability of more adsorption sites [52,53]. However, as expected, the adsorption capacity decreased with an increase in adsorbent mass, due to the reduction in effective surface area and adsorbate/adsorbent ratio [54,55].

3. Effect of pH

Generally, solution pH can affect the surface charge of the adsorbent, the degree of ionization of the material present in the aqueous system, the dissociation of functional groups on the active sites of the adsorbent, and the chemistry of dye solution [56].

The effect of the initial pH on the adsorption of the BR 18 dye solution onto the nanoclay was studied in the pH range of 3.0-10.0 with a fixed adsorbent concentration (0.04 g in 200.0 mL of 20.0 mg L^{-1} of dye solution). The pH value of the initial dye solu-

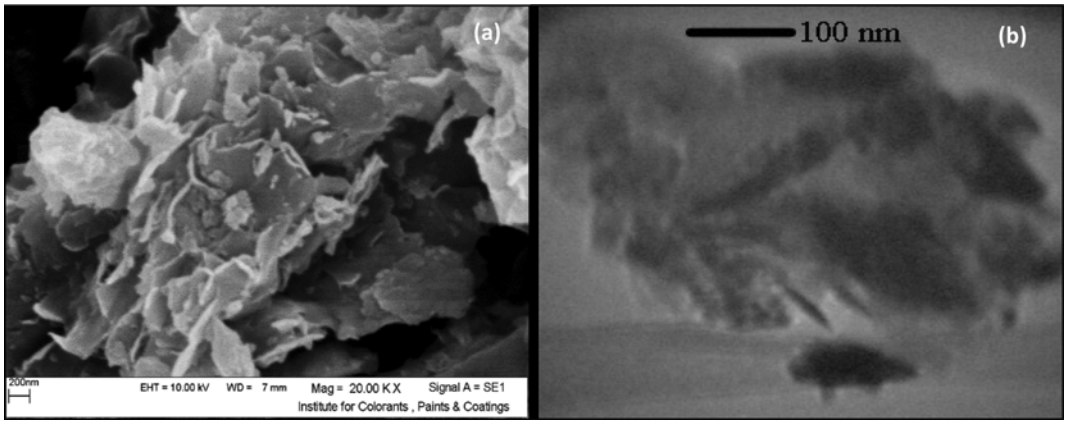

Fig. 3. (a) SEM image of montmorillonite (b) TEM micrograph of montmorillonite.

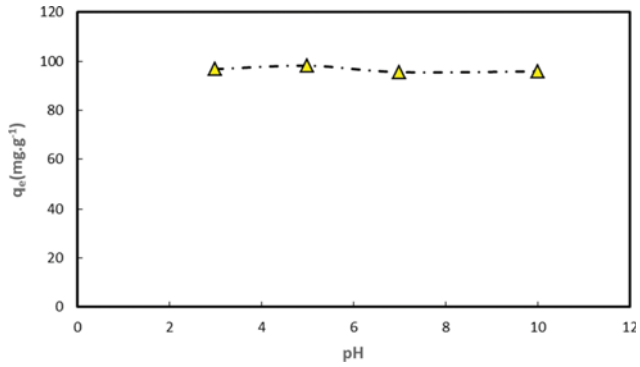

Fig. 5. Effect of pH on the adsorption of BR 18 (Condition: M=0.04 g, T=25±1 °C, C_0=20 mg L^{-1}, equilibrium time=20 min and stirring speed=200 rpm).

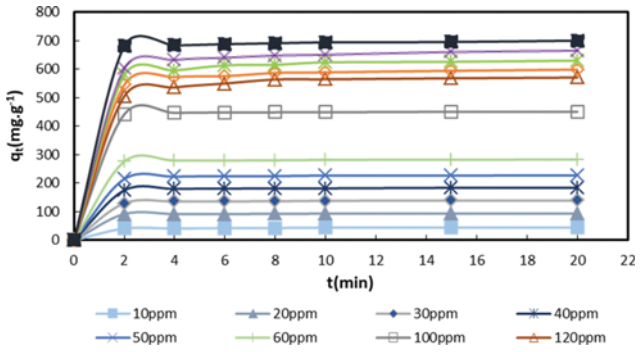

Fig. 7. Effect of Dye concentration on the adsorption of BR 18 (Condition: pH=4.8, M=0.04 g, T=25±1°, equilibrium time=20 min and stirring speed=200 rpm).

tion was adjusted using a 0.1 M HCl or NaOH solution. Nanoclay was then added to the solution and agitated for enough time to attain equilibrium.

It is expected that the amount of BR 18 adsorption will decrease in acidic pH, due to electrostatic repulsion and competitive sorption between H^+ and BR 18 cations. But, as Fig. 5 shows, the solution pH in the range of 3-10 did not affect the BR 18 adsorption by nanoclay. This means that BR 18 removal from the solution is almost independent of pH because of higher adsorption capacities of montmorillonite. In addition, BR 18 adsorption occurs quickly due to a higher number of montmorillonite active sites. This type of the surface reaction is very similar to ion exchange process [57,58].

4. Effect of Agitation Speed

Agitation is an important parameter in adsorption phenomena. It can influence on the distribution of the solute in the bulk solution. Also, it can result in the formation of the external boundary film [59]. Adsorption studies were carried out at optimum pH and adsorbent dosage (pH=4.8 and M=0.04 g) and for dye initial concentration of 20 mg/L. The stirring speed varied from 30 to 200 rpm. Samples were taken at equilibrium time and analyzed for BR 18 concentration in solution.

Fig. 6 shows the amount of BR 18 adsorbed using nanoclay at different agitation speed for contact time of 20 min. As can be seen, one can say that stirring speed had no a significant effect on adsorption rate. Therefore, a stirring speed of 200 rpm was considered for further experiments.

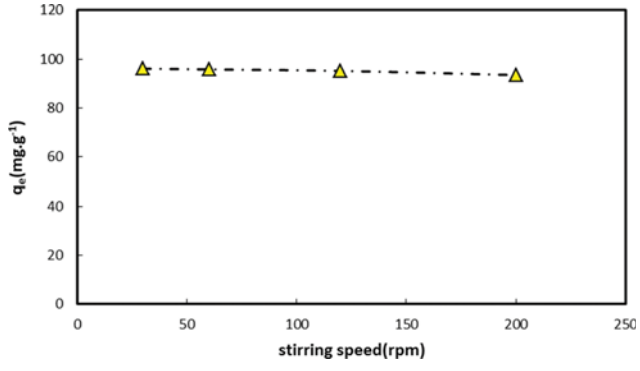

Fig. 6. Effect of stirring speed on the adsorption of BR 18 (Condition: pH=4.8, M=0.04 g, T=25±1 °C, C_0=20 mg L^{-1} and equilibrium time=20 min).

5. Dye Concentration and Contact Time

The influence of dye concentration on adsorption percentage of dye was investigated at a range of 10-200 mg·L^{-1}. The experiments were carried out at optimum adsorbent dose (0.04 g/200 ml) in the test solution, temperature (25±1 °C), pH (4.8) and for different time intervals (2, 4, 6, 8, 10, 15, and 20 min).

From Fig. 7, it is observed that the uptake of dye onto nanoclay increased rapidly at the early stages of adsorption process, followed by a gradual increase again and then decreased gradually until equilibrium was reached. Similar result was reported by Anirudhan et al. in the case of the adsorption of basic dyes onto modified bentonite clay [60]. The time required to reach equilibrium was 20 min. The amount of BR 18 dye adsorbed at equilibrium was 93.5 mg·g^{-1} (94.35%) at an initial concentration of 20 mg/L and a pH of 4.8 at 25±1 °C. The high efficiency in uptake at the initial stages was due to the high availability of adsorption sites on the surface of nanoclay. After a rapid uptake, a transitional phase occurred in which the rate of removal was slow and then reached a constant value.

Fig. 7 further shows that the increase in dye concentration increased the dye removal. When the concentration was increased from 10 to 200 mg/L, the amount of removal increased from 44.72 to 700.73 mg·g^{-1}. From this one can say that BR 18 dye uptake is highly dependent on concentration of the adsorbate.

6. Effect of Temperature

A study of the temperature dependence of adsorption reaction gives valuable knowledge about the enthalpy and entropy changes during adsorption. The removal of BR 18 onto nanoclay was studied at 298, 308, and 318 K to determine the thermo-dynamic parameters such as changes in Gibbs energy ΔG^0 (kJ·mol^{-1}), enthalpy change ΔH^0 (kJ·mol^{-1}), and entropy change ΔS^0 (J·mol^{-1} K^{-1}).

Fig. 8 shows the relationship between the amount of dye adsorbed per unit mass of adsorbent and solution temperature. The adsorption capacity rose from 93.5 to 97 mg·g^{-1} with an increase in temperature, due to a greater number of molecules to acquire sufficient energy to undergo an interaction with active sites on the adsorbent surface [61].

7. Isotherm Studies

When the dye concentration was increased from 10 to 100 mg·

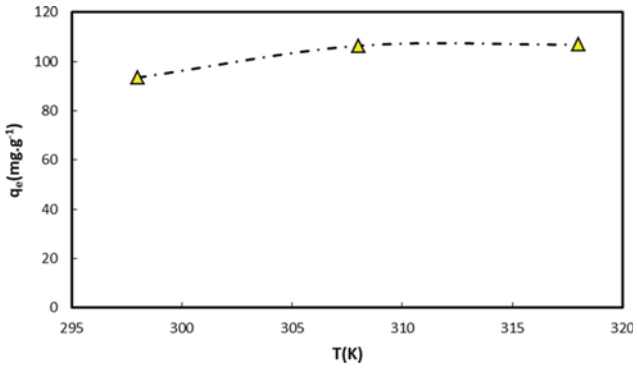

Fig. 8. Effect of temperature on the adsorption of BR 18 (Condition: pH=4.8, M=0.04 g, C_0=20 mg L^{-1}, equilibrium time=20 min and stirring speed=200 rpm).

L^{-1}, the rate of dye adsorbed kept basically unchanged and fluctuated between 94.3 and 99.4 (%). So, to perform isotherm studies, the dye concentration was varied in the range of 100-200 mg·L^{-1}. The parameters of isotherm models are given in Table 1. The adsorption isotherm of the BR 18 dye onto the nanoclay is shown in Fig. 9.

According to Table 1 and the R^2 values, the experimental equilibrium data have a good agreement with both Langmuir and Freundlich models; however, the adsorption data fit the Langmuir model better than the Freundlich and Temkin models. The Langmuir model was preferred due to the physical meaning attributed to its constants, particularly q_m, which is used for the discussion of results on the basis of the chemical properties of samples. Also, the adsorption isotherms fitted well the Langmuir model in comparison to Freundlich one, which indicates that the adsorption of BR 18 on the surface of montmorillonite is monolayer. Similar results were observed in the isotherm experiment of Methylene blue on broad bean peels [62] and Reactive red 241 and Acid blue 113 on activate carbon [63].

Moreover, based on the R_L value (presented in Table 1), the adsorption of the dye onto the nanoclay is favorable, which suggests that adsorption occurs on the homogeneous surface of the adsorbent with identical binding positions.

8. Kinetic Studies

The kinetic parameters of different models are given in Table 2. As can be seen, pseudo-second-order expression shows the highest correlation (R^2=1.00) than the other kinetic models, which indicates that the adsorption of BR18 onto nanoclay follows a pseudo-second-order kinetic model. The values of k_2 and q_e were determined experimentally from the slope and intercept of a plot of t/q_t versus t (Fig. 10). According to the assumptions of pseudo-second-order model, adsorption involves various mechanisms comprising chemical and electrostatic interactions between adsorbate molecules and functional groups on the adsorbent surface [64].

The values of k_1 and q_e were obtained from the slope and intercept of log (q_e–q_t) versus t plot, respectively [65]. It is obvious from

Table 1. The Freundlich, Langmuir and Temkin adsorption isotherm constants

Dye	Langmuir isotherm				Freundlich isotherm			Temkin isotherm		
	Q_0	K_L	R_L	R^2	K_F	n	R^2	K_1	K_2	R^2
BR 18	714.3	0.5	0.09	0.9963	457.1	10.55	0.9891	50.44	10216.36	0.96

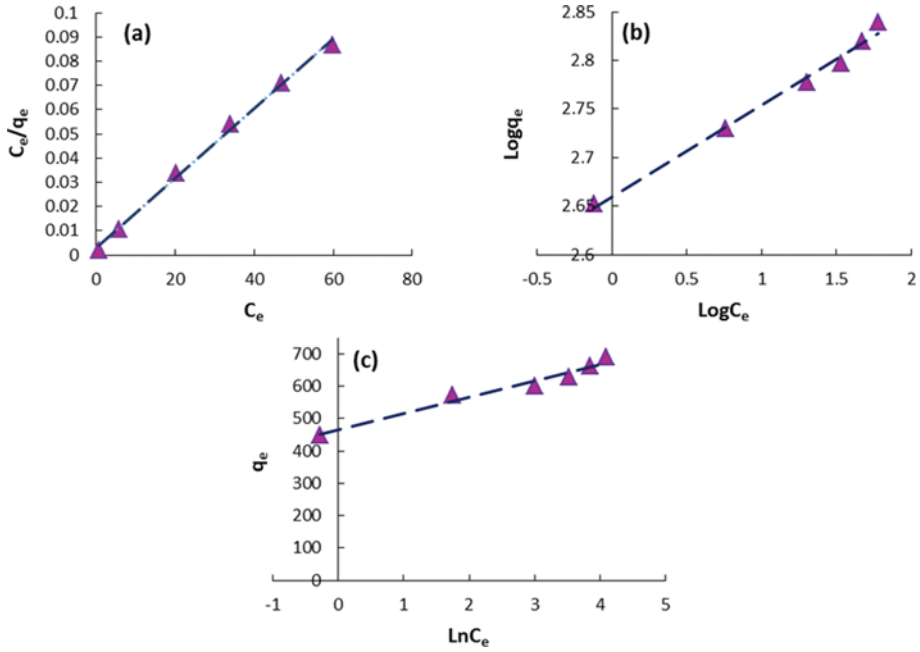

Fig. 9. Adsorption isotherms of BR 18 on nanoclay at T=25±1°, (a) Langmuir, (b) Freundlich, (c) Temkin isotherm models.

Table 2. The parameters of pseudo-first-order, pseudo-second-order and intra-particle diffusion kinetic models

C_0	Pseudo-first-order model				Pseudo-second-order model			Intra-particle diffusion model	
	$q_{e,exp}$	$q_{e,cal}$	K_1	R^2	$q_{e,cal}$	K_2	R^2	$K_{i,1}$	$K_{i,2}$
100	451.1	15.5	0.2797	0.9060	454.5	0.0484	1	6.2684	1.3389
120	571.2	88.6	0.2584	0.9418	588.2	0.0058	1	40.859	4.2976
140	598.9	65.7	0.1933	0.9729	588.2	0.0073	1	27.815	7.0811
160	630.5	68.6	0.2053	0.9457	625.0	0.0064	1	32.537	8.2910
180	665.6	79.5	0.1850	0.9834	666.7	0.0056	1	37.332	12.063
200	700.7	24.3	0.1170	0.9600	714.3	0.0098	1	6.3380	-

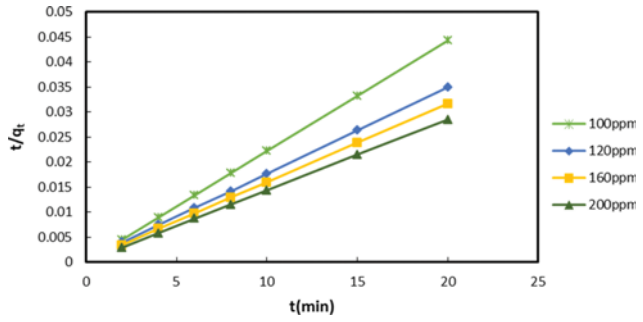

Fig. 10. Pseudo-second-order kinetics for the adsorption of BR 18 onto nanoclay (Condition: pH=4.8, T=25±1°, M=0.04 g, C_0= 20 mg·L^{-1}, equilibrium time=20 min and stirring speed= 200 rpm).

Table 2 that the calculated q_e values did not agree with the experimental q_e values. Thus, the pseudo-first-order model did not fit well.

Intra-particle diffusion model based on the theory proposed by Weber and Morris was attempted to identify the diffusion mechanism, and C_b and K_p were obtained from the slope and intercept of the straight line of q_t versus $t^{1/2}$, respectively (Fig. 11).

The intra-particle diffusion model usually includes three steps. The first, sharper portion, is the instantaneous adsorption or external surface adsorption. The second portion represents the gradual adsorption stage where intra-particle diffusion is the rate-limiting process. The third portion may exist in some cases, which denotes the final equilibrium stage where intra-particle diffusion begins to decelerate due to the highly low adsorbate concentrations left in the solution phase [64]. Fig. 11 shows that the linear plot did not pass through the origin, which indicates that the intra-particle diffusion was not the only rate-controlling step and the boundary layer diffusion governed the adsorption to some degree. According to Mahmoud et al. [66], this deviation may be due to the difference in mass transfer rate in the early and final stages of adsorption process. The values of the intercept C increased with an growth in initial dye concentration (100 to 200 mg·L^{-1}), which indicated an increasing boundary layer influence.

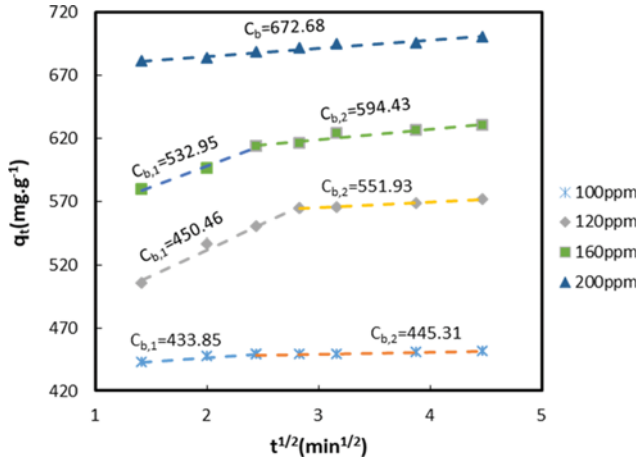

Fig. 11. Intra-particle diffusion model for adsorption of BR 18 onto nanoclay (Condition: pH=4.8, T=25±1°, M=0.04 g, C_0=20 mg·L^{-1}, equilibrium time=20 min and stirring speed=200 rpm).

In this study, adsorption mechanism was independent of stirring speed changes, so the intra-particle diffusion model was also independent of the change in stirring speed. The intra-particle diffusion model of BR 18 adsorption on montmorillonite depends on initial concentration. Similar phenomena were observed in the kinetic experiments of Methylene blue on kaolin [42] and maxilon blue 5G on sepiolite [11].

9. Adsorption Thermodynamics

Thermodynamic parameters of the adsorption process were calculated using Eqs. (11) and (12) (Table 3). ΔG^0 values were negative at all investigated temperatures, describing the spontaneous nature of adsorption of BR 18 onto nanoclay [67]. The positive value of ΔH^0 further confirms the endothermic nature of the adsorption process and shows high value of reaction heat (35.22 kJ/mol). It indicates that the temperatures slightly above the ambient would be favorable to conduct the BR 18 adsorption. The positive ΔS value shows an increased randomness of the adsorbed dye molecules on nanoclay surface [68].

10. Adsorption Modelling

As mentioned, a pseudo-second-order model can well describe the kinetic of adsorption process. Taking the kinetic rate into account, Eq. (14) is simplified to:

Table 3. Thermodynamic parameters for adsorption of BR 18 onto nanoclay (Condition: M=0.04 g/200 ml, t=20 min and C_0= 20 mg·g^{-1})

Dye	ΔG (kj/mol)			ΔH	ΔS	R^2
	298	308	318	(kj/mol)	(J/mol·K)	
BR 18	−3.87	−5.43	−6.99	35.22	156.09	0.9104

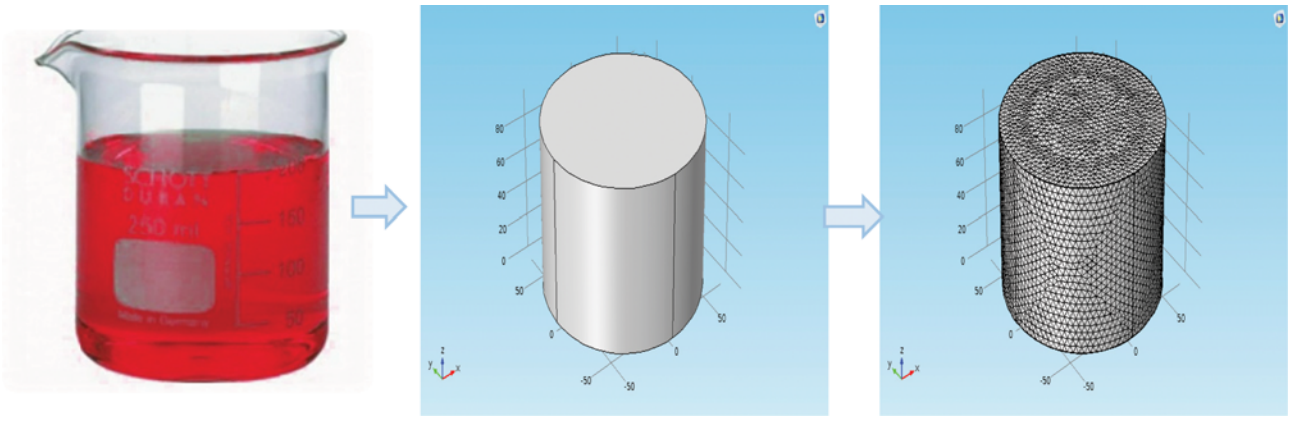

Fig. 12. The finite element model of a batch system.

$$\frac{\partial C}{\partial t} = \nabla \cdot (D_{diff} \nabla \cdot C) - \rho Y \tag{15}$$

Considering that i-component participates in the reaction process, then:

$$\rho Y = \sum_{i=1}^{i} k_i C_i^p \tag{16}$$

where P indicates the order of the reaction, and k_i represents the kinetic rate constant. It is assumed that the kinetic of dye adsorption on solid surfaces is almost identical to the rate of concentration change in solution phase ($\partial C/\partial t$) [69]. Substituting Eq. (8) into Eq. (15) yields the following equation:

$$\frac{\partial C}{\partial t} = \nabla \cdot (D_{diff} \nabla \cdot C) - K_2 (q_e - q_t)^2 \tag{17}$$

Considering Eq. (1) and Eq. (6), Eq. (17) can be now rewritten as:

$$\frac{\partial C}{\partial t} = \nabla \cdot (D_{diff} \nabla \cdot C) - K_2 \cdot b \cdot (C_t - C_e)^2 \tag{18}$$

where b is a constant which depends on the volume of the solution and the amount of adsorbent.

11. Definition of Physical Laws and Equations in COMSOL Multiphysics

The transport of diluted species (tds) was chosen for this modelling. In the mass transfer mode, COMSOL Multiphysics allows the user to apply the general mass transport equation (Eq. (19)). The user must provide the numerical values or expressions for the constants in the model such as diffusion coefficient [70].

$$\frac{\partial C_i}{\partial t} + \nabla \cdot (-D_i \nabla \cdot C_i) = R_i - u \nabla \cdot C_i \tag{19}$$

where D_i represents diffusion coefficient, R_i and u are chemical reaction term and convection process, respectively.

Table 4. The equivalent of defined model and COMSOL coefficients

COMSOL coefficients	Defined model
D_i	D_{diff}
R_i	$-K_2 \cdot b \cdot (C_t - C_e)^2$

12. The Equivalent of Defined Model (Eq. (18)) and COMSOL Coefficients

Adsorption is a mass transfer reaction that converts BR 18 from a dissolved state into an adsorbed state. Table 4 relates the COMSOL coefficients (Eq. (19)) with the equivalent term in defined model (Eq. (18)).

13. Modelling Setting and Input Data

To model the adsorption process, a three-dimensional geometry was first built using COMSOL Multiphysics. The radius and height of a one-dimensional finite element model were 75 mm and 95 mm, respectively (Fig. 12). It was assumed that the adsorption takes place in a batch system.

A molecular diffusion coefficient of 1×10^{-8} m^2/s was assigned for BR 18 dye in the solution phase [69]. An initial condition equal to dye initial concentration in the aqueous system was specified in order to solve model equation governing the adsorption process numerically.

Fig. 13 compares the dye concentrations in solution system versus time and as a function of dye concentration predicted by the numerical finite element model (solid lines) and experimental data (dots). As Fig. 13 shows, an excellent agreement was achieved. Both numerical model and experimental data show that BR 18 dye re-

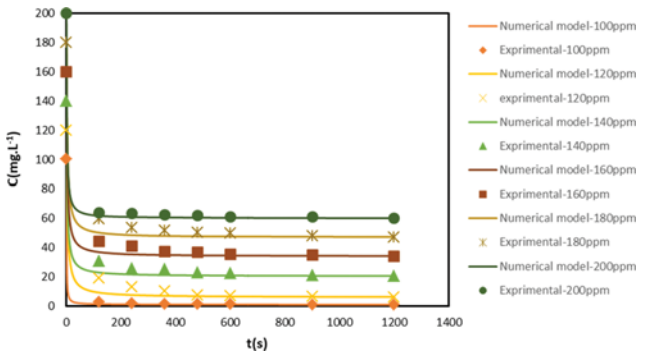

Fig. 13. Comparison of the concentrations of BR 18 dye in aqueous phase versus time predicted by the numerical model (solid lines) and determined at laboratory (dots) (Condition: pH= 4.7, stirring speed=200 rpm, T=25±°C, C_0=100-200 mg·L^{-1} and M=0.04 g).

moval by nanoclay occurred fast in the early stages of adsorption process.

CONCLUSIONS

The application of montmorillonite for adsorption of the Basic Red 18 dye in aqueous solutions was investigated. The adsorption was highly dependent on various operating parameters such as adsorbent dose, contact time, dye initial concentration and temperature. Increase in the dye initial concentration and temperature enhanced the interaction between dye and nanoclay, resulting in greater adsorption capacity.

The equilibrium analysis showed that the Langmuir isotherm yielded a better fit to the adsorption data, signifying that the BR 18 forms a monolayer on the adsorbent. The pseudo-second-order model showed the best correlation for the experimental data. The results of intra-particle diffusion model revealed that intra-particle diffusion is not the only process controlling the BR 18 adsorption on nanoclay. Thermodynamic parameters suggest that the adsorption is spontaneous and endothermic. Montmorillonite resulted in a maximum adsorption of 714.3 mg g^{-1} for BR 18 dye. The high adsorption capacity, less pH sensitivity and thermodynamic stability of nanoclay showed that this adsorbent can be used as an alternative for removal of BR 18 dye from industrial wastewater.

Adsorption modelling is important in developing an appropriate treatment system and controlling pollution load discharging to the environment. BR 18 adsorption was modelled using COMSOL Multiphysics. The model was homogeneous and included diffusion term and kinetics expression. The predicted outputs of the model were in close agreement with the experimental data.

REFERENCES

1. D. Bingöl, S. Veli, S. Zor and U. Özdemir, *Synthetic Metals*, **162**, 1566 (2012).
2. Q. Liu, B. Yang, L. Zhang and R. Huang, *Int. J. Biological Macromolecules*, **72**, 1129 (2015).
3. R. Sivashankar, A. Sathya, K. Vasantharaj and V. Sivasubramanian, *Environ. Nanotechnol., Monitoring Manage.*, **1**, 36 (2014).
4. M. Gholami, M. Shirzad-Siboni and J.-K. Yang, *Korean J. Chem. Eng.*, **33**, 812 (2016).
5. S. Afroze, T. K. Sen and H. Ang, *Research on Chemical Intermediates*, **42**, 2343 (2016).
6. T. Robinson, B. Chandran and P. Nigam, *Environ. International*, **28**, 29 (2002).
7. T. Robinson, G. McMullan, R. Marchant and P. Nigam, *Bioresour. Technol.*, **77**, 247 (2001).
8. F. Mateen, I. Javed, U. Rafique, N. Tabassum, M. Sarfraz, S. Z. Safi, I. Yusoff and M. A. Ashraf, *Desalination and Water Treatment*, **57**, 6230 (2016).
9. M. Rafatullah, O. Sulaiman, R. Hashim and A. Ahmad, *J. Hazard. Mater.*, **177**, 70 (2010).
10. M. Toor and B. Jin, *Chem. Eng. J.*, **187**, 79 (2012).
11. M. Alkan, M. Doğan, Y. Turhan, Ö. Demirbaş and P. Turan, *Chem. Eng. J.*, **139**, 213 (2008).
12. S. Haddadi Khorzughy, T. Eslamkish, F. Doulati Ardejani and M. R. Heydartaemeh, *Korean J. Chem. Eng.*, **32**, 88 (2015).
13. T. Sismanoglu and A. Z. Aroguz, *Desalination and Water Treatment*, **54**, 736 (2015).
14. B. Acevedo, R. P. Rocha, M. F. Pereira, J. L. Figueiredo and C. Barriocanal, *J. Colloid Interface Sci.*, **459**, 189 (2015).
15. N. Abidi, E. Errais, J. Duplay, A. Berez, A. Jrad, G. Schäfer, M. Ghazi, K. Semhi and M. Trabelsi-Ayadi, *J. Cleaner Production*, **86**, 432 (2015).
16. M. Auta and B. H. Hameed, *Environ. Eng. Manage. J.*, **14**, 955 (2015).
17. K. Bennani, B. Mounir, M. Hachkar, M. Bakasse and A. Yaacoubi, *J. Mater. Environ. Sci.*, **6**, 2483 (2015).
18. Y.-M. Chen, T.-M. Tsao, M.-K. Wang, S. Yu, C.-C. Liu, H.-C. Li, C.-Y. Chiu and L.-C. Wang, *Water Environ. Res.*, **87**, 88 (2015).
19. P. Liu and L. Zhang, *Sep. Purif. Technol.*, **58**, 32 (2007).
20. S. C. Santos and R. A. Boaventura, *J. Environ. Chem. Eng.*, **4**, 1473 (2016).
21. A. M. Bandpei, S. M. Mohseni, A. Sheikhmohammadi, M. Sardar, M. Sarkhosh, M. Almasian, M. Avazpour, Z. Mosallanejad, Z. Atafar and S. Nazari, *Korean J. Chem. Eng.*, 1 (2015).
22. C.-Y. Ryu and S.-D. Yeo, *Korean J. Chem. Eng.*, **27**, 602 (2010).
23. G. K. Sarma, S. S. Gupta and K. G. Bhattacharyya, *J. Environ. Manage.*, **171**, 1 (2016).
24. J. Ahmadishoar, H. S. Bahrami, B. Movassagh, H. S. Amirshahi and M. Arami, *Chem. Industry Chem. Eng. Quarterly*, 49 (2016).
25. L. Ma, Y. Xi, H. He, G. A. Ayoko, R. Zhu and J. Zhu, *Appl. Clay Sci.*, **120**, 9 (2016).
26. H. Hosseinzadeh and N. Khoshnood, *Desalination and Water Treatment*, **57**, 6372 (2016).
27. B. A. Fil, *Particulate Sci. Technol.*, **34**, 118 (2016).
28. F. Doulati Ardejani, K. Badii, N. Y. Limaee, N. Mahmoodi, M. Arami, S. Shafaei and A. Mirhabibi, *Dyes Pigments*, **73**, 178 (2007).
29. M. Ghadiri, M. Asadollahzadeh and A. Hemmati, *J. Water Process Eng.*, **6**, 144 (2015).
30. J. Xiao, Y. Liu, J. Wang, P. Bénard and R. Chahine, *Int. J. Heat Mass Transfer.*, **55**, 6864 (2012).
31. Q. Li, K. Ito, Z. Wu, C. S. Lowry, I. Loheide and P. Steven, *Ground Water*, **47**, 480 (2009).
32. W. Qian, J. Wu, L. Yang, X. Lin, Y. Chen, X. Chen, J. Xiong, J. Bai and H. Ying, *Chem. Eng. J.*, **197**, 424 (2012).
33. L. Wissmeier and D. A. Barry, *Environ. Modelling Software*, **26**, 210 (2011).
34. S. Netpradit, P. Thiravetyan and S. Towprayoon, *Water Res.*, **37**, 763 (2003).
35. I. Langmuir, *J. American Chem. Soc.*, **38**, 2221 (1916).
36. S. S. Abkenar, R. M. A. Malek and F. Mazaheri, *J. Environ. Manage.*, **163**, 53 (2015).
37. H. Freundlich, *J. Phys. Chem.*, **57**, 1100 (1906).
38. A. Mittal, D. Jhare and J. Mittal, *J. Mole. Liq.*, **179**, 133 (2013).
39. M. Auta and B. Hameed, *Chem. Eng. J.*, **198**, 219 (2012).
40. M. Mostafa, Y.-H. Chen, J.-S. Jean, C.-C. Liu and Y.-C. Lee, *J. Hazard. Mater.*, **187**, 89 (2011).
41. Y.-S. Ho and G. McKay, *Process Biochem.*, **34**, 451 (1999).
42. K. Rida, S. Bouraoui and S. Hadnine, *Appl. Clay Sci.*, **83**, 99 (2013).
43. W. J. Weber and J. C. Morris, *J. Sanitary Eng. Division*, **89**, 31 (1963).
44. L. Wang, *J. Environ. Manage.*, **102**, 79 (2012).
45. B. A. Robinson, Z. Lu and D. Pasqualini, *Applied Mathematics*, **3**,

1161 (2012).
46. I. Bortone, A. Di Nardo, M. Di Natale, A. Erto, D. Musmarra and G. Santonastaso, *J. Hazard. Mater.*, **260**, 914 (2013).
47. P. S. Nayak and B. Singh, *Bulletin Mater. Sci.*, **30**, 235 (2007).
48. G. Lv, Z. Li, W.-T. Jiang, P.-H. Chang and L. Liao, *Mater. Chem. Phys.*, **162**, 417 (2015).
49. D. Liu, P. Yuan, H. Liu, J. Cai, D. Tan, H. He, J. Zhu and T. Chen, *Appl. Clay Sci.*, **80**, 407 (2013).
50. A. Hassani, M. Kiranşan, R. D. C. Soltani, A. Khataee and S. Karaca, *Turkish J. Chem.*, **39**, 734 (2015).
51. M. Grieve, R. Griffin and R. Malone, *Sci. Justice*, **38**, 27 (1998).
52. V. Venkateswaran, P. Kalaamani and N. Karpagam, *Chem. Sci. Transaction*, **4**, 347 (2015).
53. V. K. Garg, M. Amita, R. Kumar and R. Gupta, *Dyes Pigments*, **63**, 243 (2004).
54. F. Nekouei, S. Nekouei, I. Tyagi and V. K. Gupta, *J. Mole. Liq.*, **201**, 124 (2015).
55. B. Tanhaei, A. Ayati, M. Lahtinen and M. Sillanpää, *Chem. Eng. J.*, **259**, 1 (2015).
56. A. Tehrani-Bagha, H. Nikkar, N. Mahmoodi, M. Markazi and F. Menger, *Desalination*, **266**, 274 (2011).
57. O. Duman, S. Tunc and T. G. Polat, *Micropor. Mesopor. Mater.*, **210**, 176 (2015).
58. V. Garg, R. Gupta, A. B. Yadav and R. Kumar, *Bioresour. Technol.*, **89**, 121 (2003).
59. B. Nandi, A. Goswami and M. Purkait, *J. Hazard. Mater.*, **161**, 387 (2009).
60. T. Anirudhan and M. Ramachandran, *Process Safety Environ. Protection*, **95**, 215 (2015).
61. K. Chinoune, K. Bentaleb, Z. Bouberka, A. Nadim and U. Maschke, *Appl. Clay Sci.*, **123**, 64 (2016).
62. B. Hameed and M. El-Khaiary, *J. Hazard. Mater.*, **154**, 639 (2008).
63. P. Faria, J. Orfao and M. Pereira, *Water Res.*, **38**, 2043 (2004).
64. I. Tan, B. Hameed and A. Ahmad, *Chem. Eng. J.*, **127**, 111 (2007).
65. A. Hassani, R. D. C. Soltani, S. Karaca and A. Khataee, *J. Ind. Eng. Chem.*, **21**, 1197 (2015).
66. D. K. Mahmoud, M. A. M. Salleh, W. A. W. A. Karim, A. Idris and Z. Z. Abidin, *Chem. Eng. J.*, **181**, 449 (2012).
67. S. Sonawane, P. Chaudhari, S. Ghodke, S. Ambade, S. Gulig, A. Mirikar and A. Bane, *Ultrasonics Sonochemistry*, **15**, 1033 (2008).
68. H. Hosseinzadeh, S. Zoroufi and G. R. Mahdavinia, *Polymer Bulletin*, **72**, 1339 (2015).
69. F. Doulati Ardejani, K. Badii, F. Farhadi, M. A. Saberi and B. J. Shokri, *Environ. Modeling Assessment*, **17**, 505 (2012).
70. J. P. Orjuela and A. González, Comsol Conference, Boston (2011).